A&A 516, A40 (2010)
DOI: 10.1051/0004-6361/200913207

Astronomy & Astrophysics

Evolution of the ISM in luminous infrared galaxies

W. A. Baan[1], A. F. Loenen[2], and M. Spaans[3]

[1] ASTRON, Oude Hoogeveensedijk 4, 7991 PD Dwingeloo, The Netherlands
e-mail: baan@astron.nl
[2] Leiden Observatory, Leiden University, PO Box 9513, 2300 RA Leiden, The Netherlands
[3] Kapteyn Astronomical Institute, PO Box 800, 9700 AV Groningen, The Netherlands

Received 29 August 2009 / Accepted 7 April 2010

ABSTRACT

Aims. Molecules that trace the high-density regions of the interstellar medium may be used to evaluate the changing physical and chemical environment during the ongoing nuclear activity in (ultra-)luminous infrared galaxies (ULIRGs).
Methods. The changing ratios of the HCN (1−0), HNC (1−0), HCO^+ (1−0), CN (1−0) and CN (2−1), and CS (3−2) transitions were compared with the HCN (1−0)/CO (1−0) ratio, which is proposed to represent the progression time scale of the starburst. These diagnostic diagrams were interpreted using the results of theoretical modeling with a large physical and chemical network to describe the state of the nuclear ISM in the evolving galaxies.
Results. Systematic changes are seen in the line ratios as the sources evolve from early stage for the nuclear starburst (ULIRGs) to later stages. These changes result from changing environmental conditions and particularly from the lowering of the average density of the medium. A temperature rise due to mechanical heating of the medium by feedback explains the lowering of the ratios at later evolutionary stages. Infrared pumping may affect the CN and HNC line ratios during early evolutionary stages.
Conclusions. Molecular transitions display a behavior that relates to changes of the environment during an evolving nuclear starburst. Molecular properties may be used to designate the evolutionary stage of the nuclear starburst. The HCN(1−0)/CO(1−0) and HCO^+(1−0)/HCN(1−0) ratios serve as indicators of the time evolution of the outburst.

Key words. infrared: galaxies – ISM: molecules – radio lines: galaxies – galaxies: active – galaxies: starburst

1. Introduction

The (ultra-)luminous infrared galaxies (ULIRGs) are powered by a (circum-)nuclear starburst and/or an active galactic nucleus (AGN). ULIRGs belong to a much larger population of submillimeter galaxies (SMGs) that peaks at redshift 2−3 and extends to $z = \sim 6$. The relatively short episodes of intense nuclear activity in ULIRGs and SMGs have likely been triggered by galaxy mergers or collisions, which produce the most luminous galaxies in the universe.

Among other spectral observations, the emissions from the high-density molecular material in the nuclear region of external galaxies allow a clear view of the ISM and are a preferred tool for diagnosing the physical and chemical environment of the starforming and AGN-excited ISM. A strong relation has been found between the far-infrared luminosity and the luminosity of molecular emissions, that are indicators of the high-density ($n(H_2) \gtrsim 10^{4-6}\,cm^{-3}$) component of the interstellar medium (Gao & Solomon 2004; Curran et al. 2000; Baan et al. 2008). Since these integrated emissions predominantly arise from the nuclear region, they are closely associated with the nuclear starburst/AGN environment and the production of the FIR and submillimeter luminosities.

Each molecular species responds differently to the changing physical and chemical environment of the nuclear region. The collective behavior of molecular tracers may thus be used to characterize the evolution of the nuclear environment during a nuclear activity. In this paper, we consider evolutionary changes of the ISM as seen by the molecular tracer emissions and resulting from the ongoing star-formation, the AGN activity, and any feedback processes. Diagnostic interpretation of the behavior of molecular line ratios is based on theoretical modeling using a large physical and chemical network to describe the state of the nuclear ISM in the evolving galaxies.

This study considers mostly single molecular transitions for the multi-molecular modeling. The inclusion of multiple higher transitions will augment the diagnostic accuracy of the modeling analysis. Modeling of the observed ground state transitions already predicts the behavior of higher transitions and their ratios and will be used in future work to incorporate newly obtained observational data and data expected from Herschel and ALMA.

2. Modeling the evolving ISM

The emissions of molecular species observed in active nuclei are determined by their chemical abundances, the density and temperature of the medium, their column density, and the excitation conditions in the ISM. While multiple level studies of single molecules may be used to reveal the density and/or kinetic temperature of ISM components, the ensemble of emissions of tracer molecules will diagnose the dominant physical and chemical properties of the environment.

2.1. Modeling the evolution of a starburst

The observed nearly linear relations between the emission luminosity of high-density tracers and the far-infrared luminosity (FIR) represent the response of the nuclear medium to the activity in the evolving nucleus (Gao & Solomon 2004; Curran et al. 2000; Baan et al. 2008). The star-formation that generates

the FIR luminosity also proportionally depletes and destroys the high-density (HD) component of the nuclear ISM, and the HD line emission decreases in time. The low-density (LD) component, however, is not involved in the star-formation process and will remain (largely) the same. For this reason, the changing HD/LD ratio during a nuclear outburst may serve as an indicator of the evolutionary age of the outburst. In Sect. 2.3, it will be proposed to use the HCN (1−0)/CO (1−0) line emission ratio as an indicator of the HD/LD emission ratio and the evolutionary stage of the starburst.

The time evolution of the FIR luminosity of a nuclear starburst may be characterized by a rapid rise to a peak luminosity followed by an exponential tail (Loenen et al. 2006; Baan et al. 2008). In order to obtain further understanding about the FIR evolution and the HD-depletion during a starburst, we consider a simple simulation where during each time interval a fixed depletion fraction $f_{\rm dep}$ of the high-density medium is used and destroyed by the star-formation process. The HD mass component used for star-formation diminishes steadily with each timestep as:

$$\mathrm{d}M_{\rm HD}(t) = M_{\rm HD}(t-1) * f_{\rm dep}. \quad (1)$$

The FIR-luminosity follows from a time-delayed (diffusion-like) response from each of the mass fractions used in the star-formation process during earlier time intervals. This function may be defined as:

$$L_{\rm FIR}(t) = L_{\rm FIRm} \sum_{t_{\rm i}=0}^{t} \mathrm{d}M_{\rm HD}(t_{\rm i}) \left(\frac{T}{t-t_i}\right)^{2.5} \mathrm{e}^{-T/(t-t_i)}, \quad (2)$$

where $L_{\rm FIRm}$ is the maximum luminosity and T is the characteristic luminosity diffusion timescale of the burst.

The FIR-luminosity trails the mass-consumption in time, which is consistent with reality where lower mass stars have a delayed impact on the FIR-luminosity. This simulation differs from the one presented earlier in Baan et al. (2008) because here the depletion of the HD material is used to determine the FIR-luminosity, while previously the HD-depletion was deduced from the magnitude of the FIR-luminosity.

The decaying $L_{\rm FIR}$ luminosity curve is determined by the peak luminosity, the HD depletion rate per time interval, and the delay-time-scale T for the production of the FIR luminosity. The starburst simulations depicted in Fig. 1 are for three star-formation scenarios, respectively red, green, and blue curves, with initial values for the HD/LD ratio (0.2, 0.15, and 0.1), the depletion fraction $f_{\rm dep}$ per timestep (6%, 4% and 2%), and the peak luminosity ($10^{12.3}$, $10^{11.5}$, and $10^{10.6}\,L_{\odot}$). As mentioned before, the mass of the low-density component is assumed to remain unchanged. The luminosity diffusion timescale of the burst T is set equal to 2.5 timesteps. Assuming a 10^8 yr duration for the outburst, each time-step in the simulation has an approximate duration of 5×10^5 yr. While the scaling of the number and the FIR-luminosity is still arbitrary, the curves may be compared with observations.

The predicted behavior of the simulated starbursts is presented in the graphs of Fig. 1. They (expectedly) show that more rapid HD-consumption (red curve in frame b) also produces a more pronounced luminosity curve and a faster luminosity decay (frame a). The continuing reduction of the HD/LD is plotted as function of FIR-luminosity in frame c). Because of the decreasing HD consumption over time and the delay in the FIR production, the predicted number of sources in Frame d) increases towards lower values of $L_{\rm HD}/L_{\rm LD}$. The diagrams in frames c) and d) may be compared with observational data in order to test the validity of the modeling, as presented in Sect. 2.3 below.

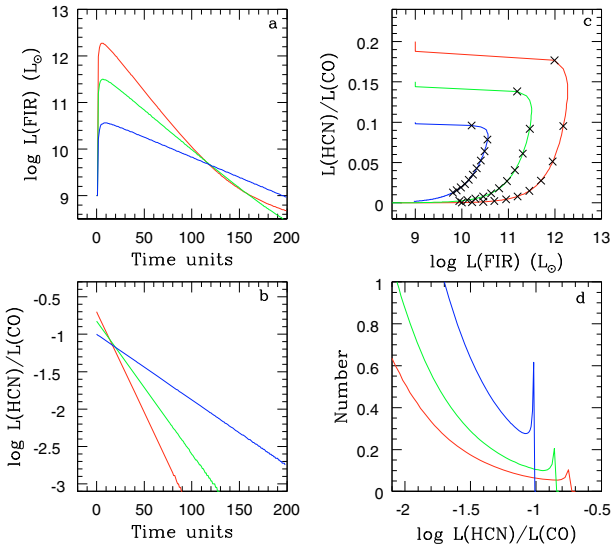

Fig. 1. Simulations of a starburst. Three initial conditions are considered (see text) and the curves are color coded. **a)** The variation of the FIR-luminosity with representative time units of 5×10^5 yr. **b)** The constant percentage-wise depletion of the high-density (HD) component relative to the low-density (LD) component. **c)** The depletion of the high-density component as a function of the FIR-luminosity. The crosses indicate intervals of 10 time-steps. **d)** The predicted number distribution of star-bursting FIR galaxies as a function of the HD/LD emission line ratio. The narrow spikes occur at the peak of the FIR-luminosity.

2.2. Chemical evolution of the starburst

The changing properties of the evolving nuclear environment trigger many related and simultaneous processes. After some high-density material is used to form the first generation of stars, the remaining high-density component will increasingly be affected by these stars, their UV-radiation fields, and the resulting (ultra-) compact HII regions. After the first massive stars produce supernovae and remnants, the dissipation of mechanical energy of the shocks will further raise the temperature and disperse the surrounding high-density material. Such processes will modify the formation of subsequent generations of stars and give a continually changing ISM. It should be noted that the time scales for shocks and photo-dissociation by UV-radiation are very short (10^4−10^5 yr; Bergin et al. 1998) as compared with the time scale of a standard starburst (10^7−10^8 yr; Coziol 1996).

The high-density component remaining after subsequent generations of stars in the evolving starburst will decrease in mass and luminosity and will be characterized by a systematically decreasing average density of the high density medium and increasing temperature, although regions of relatively higher density will remain. These changing conditions, as well as variation of the cosmic ray flux density and the radiation fields, will strongly influence the molecular chemistry.

Simulations using extensive physical and chemical modeling show that the observed intensity ratios of high-density tracers HCN, HNC, and HCO^+ in (most) extra-galactic sources are well represented by an environment that is dominated by Photon Dominated Regions (PDR) with densities ranging from $n\,(\mathrm{H_2}) = 10^{5.5}$ to 10^4 cm^{-3} (Loenen et al. 2008). Few sources in the current sample show characteristics suggesting X-ray

Table 1. Critial density for molecular transitions.

Molecule	Transition designation	Critical density (cm^{-3})
CO	$J = 1–0$	2.0×10^3
CO	$J = 2–1$	1.4×10^4
HCO^+	$J = 1–0$	2.2×10^5
CN	$N = 1–0$, $J = 3/2–1/2$	4.0×10^5
CS	$J = 3–2$	1.4×10^6
HCN	$J = 1–0$	3.1×10^6
HNC	$J = 1–0$	3.9×10^6
CN	$N = 2–1$, $J = 5/2–3/2$	1.9×10^7

Notes. Based on data from LAMDA database for a kinetic temperature of 60–70 K (Schöier et al. 2005).

Dominated Regions (XDR) (see Sect. 3.2). This density range confirms the densities anticipated for star-formation regions but also suggests global evolutionary changes in the nuclear environment during the course of an outburst. Because of different critical densities for the molecules, particularly the intermediate density tracer lines HCO^+ (1–0) and CN (1–0) (see Table 1) may become thermalized during early stages of evolution.

The observed intensity ratios for extra-galactic environments may serve to diagnose any global change in the density and other properties of the nuclear ISM. The expected variation of the HNC, HCO^+, and CS line ratios with HCN have been calculated using radiative transfer modeling within a physical/chemical network (see Loenen et al. 2008, 2010; Meijerink & Spaans 2005), while for CN the abundance ratio is presented. Figure 2 presents the predicted line ratios for PDR environments with three representative densities ($n(H_2) = 10^{5.5}$, $10^{5.0}$, and $10^{4.0}$ cm^{-3}). Variation of the UV-radiation fields only leads to modest changes in the line ratios, because the UV flux is largely attenuated at the high column densities where the molecules are abundant. In analogy with earlier simulations, the UV flux has been taken to be 160 erg s^{-1} cm^{-2} = 10^5 Habing units (Loenen et al. 2008), which is appropriate for starburst environments. An additional simulation curve considers the effect of additional mechanical heating resulting from feedback at a low rate of 5×10^{-20} erg s^{-1} cm^{-3} in the lowest density environment ($n(H_2) = 10^4$) based on a $SFR = 2.5\ M_\odot\ yr^{-1}$ (Loenen et al. 2008). This heats the gas to a temperature of approximately 200 K.

The predicted ratios in Fig. 2 display significant variation for a varying global density and for different column densities representing the surface and interior regions of clouds from which the observable emission emerges. For the ratios HNC/HCN, HCO^+/HCN, and CS/HCN the cloud interiors dominate the observed line ratios, while for CN the cloud surface would dominate the observed line ratio. The predicted values cover the range for the observed ratios.

2.3. HCN as a molecular indicator

The HCN molecule has been identified as the best high-density (HD) tracer to estimate the amount of high-density material and to describe the state of the starburst (see Gao & Solomon 2004; Baan et al. 2008). Extensive modeling shows that of the prominent HD-tracers, HCN is least sensitive to chemical and physical changes and may best serve as an indicator of the high-density molecular component (see Papadopoulos 2007; Loenen et al. 2007, 2008). The predicted line strength of emission lines

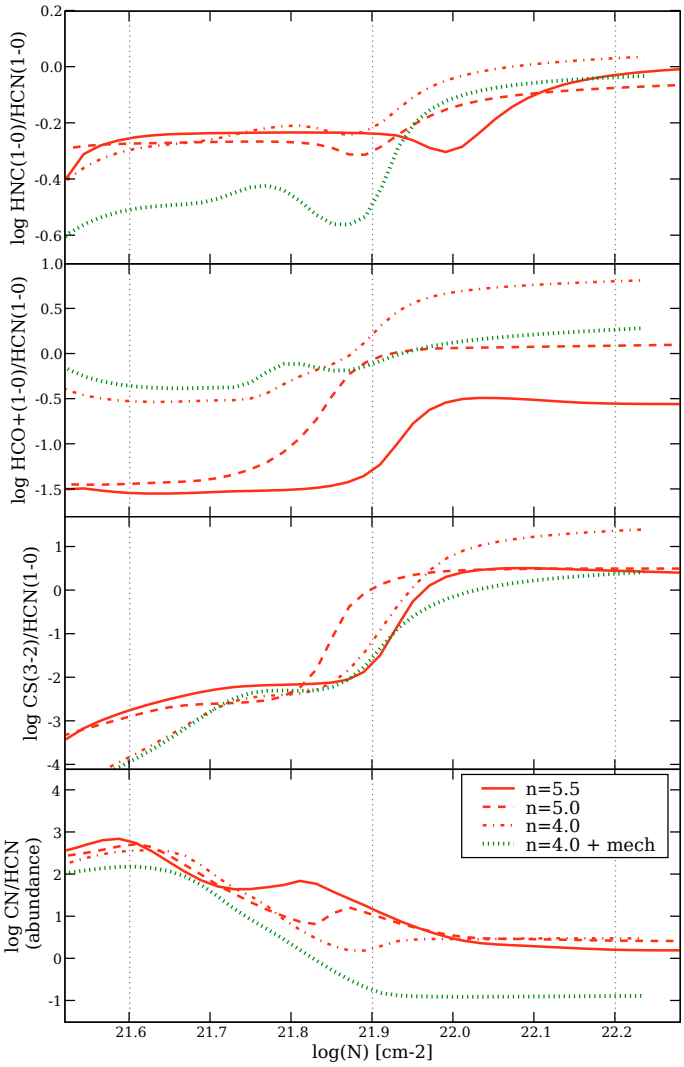

Fig. 2. Predicted line ratios for HNC (1–0)/HCN (1–0), HCO^+ (1–0)/HCN (1–0), and CS (3–2)/HCN (1–0) and the abundance ratio of CN/HCN for varying environments. The four assumed conditions represent an average density ($n = 10^n$ cm^{-3}) for the medium (red lines) and the addition of mechanical heating at the lowest density (green lines). For the CS diagram, a Sulfur depletion factor of 400 has been assumed. The vertical dotted lines designate the column density regions to be used in the discussion of the evolutionary diagrams in Sect. 3.

of HCN (1–0), HNC (1–0), and HCO^+ are presented in Fig. 3 for three densities in the range of $10^{5.5}$–10^4 cm^{-3} and for the effect of low-density mechanical heating. The physical parameters of UV-flux and mechanical heating used for the simulations are identical to those used for Fig. 2 (see Sect. 2.2).

The emission line strength in Fig. 3 varies between the cloud interior and the cloud surface and at higher densities. Furthermore, the changing ambient density may vary from above to below the critical density, which results in different excitation states for all molecules. HCN(1–0) appears less sensitive to these changes, because of its higher critical density (see Table 1), but is also quite insensitive to additional physical effects. Even though, the destruction of HNC at higher temperatures would increase the HCN abundance, this can at most only double the abundance. Mechanical heating boosts the line strength of all three molecules, but at lower densities ($n(H) = 10^4$ cm^{-3}) this merely compensates for the effect of a decrease in density. HCO^+

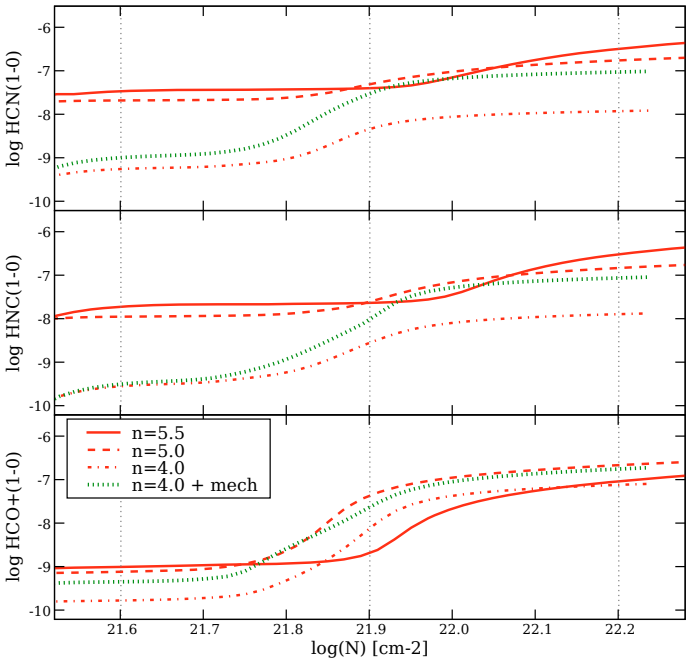

Fig. 3. Predicted line strength for HCN (1−0), HNC (1−0), and HCO^+ (1−0) for varying environments. The four assumed conditions represent an average density ($n = 10^n$ cm^{-3}) for the medium (red lines) and the addition of mechanical heating at the lowest density (green dotted lines). The vertical dotted lines designate the column density regions that will be considered in the further discussion.

might seem more stable in Fig. 3, but this is simply because the ambient density is above n_{crit} most of the time. Moreover, HCO^+ is inherently more sensitive to radiative/chemical effects, because it is an ion. Additional ionization can enhance it and higher electron abundance can destroy it.

The physical and chemical modeling does not incorporate any clumpiness of the medium, which could affect the (integrated) strength of the emission lines. However, early PDR models for a clumpy medium (Spaans 1996; Spaans & van Dishoeck 1997) indicate that opaque clumps ($A_V > 4$ mag) only modestly affect the HCN/CO ratio, which also appears applicable for a large-scale nuclear ISM. In addition, variation of the elemental abundance ratios, particularly C/N and O/N, among extragalactic sources would strongly affect the chemical balance. This would affect the strength of molecular emission lines from regions with lower column densities but not from regions with high column densities.

Although all HD tracers will vary due to changing ISM conditions, it appears that HCN is least perturbed by other physical and chemical processes of the three molecular species considered here and may well serve as a reliable indicator of the HD gas component in the source. The HCN (1−0) (and higher) line strength does not necessarily need to vary linearly with time or with FIR luminosity; it only needs to be a monotone (smooth) function of the changing environment.

The validity of HCN as a representative HD tracer has been questioned (Graciá-Carpio et al. 2006, 2008) particularly because the HCN abundance can be enhanced in the highest luminosity objects due to IR pumping (Aalto et al. 2007) and XDR chemical enhancement (Lepp & Dalgarno 1996). This XDR chemical enhancement is not depth dependent and boosts HCN over a narrow range of ionization rates and only for specific n_H and F_X (see Meijerink & Spaans 2005). Also, the XDR component will typically have a much smaller annular

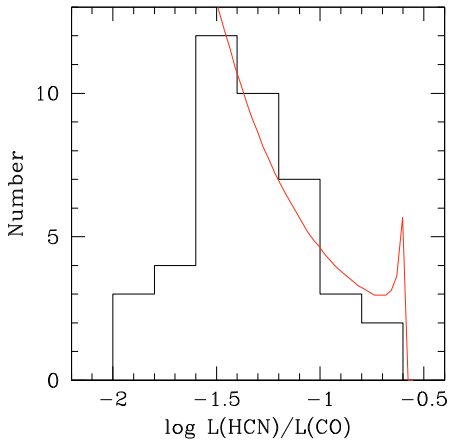

Fig. 4. A histogram of observed L(HCN)/L(CO) values versus the predicted values from simulations. The curve corresponds to the (red) prediction curve in Fig. 1c.

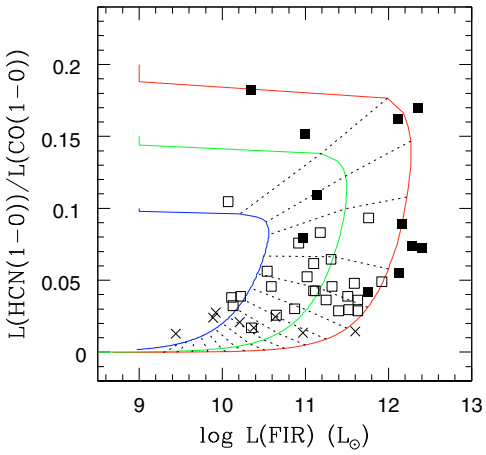

Fig. 5. Variation of the observed L(HCN)/L(CO) ratio with the FIR-luminosity predicted from simulations. The predicted starburst evolution curves for the HD/LD ratio are taken from Fig. 1c. The location of the data points may be used to estimate the evolutionary age of the starburst. Evolutionary ages are indicated with dotted lines starting from the top at timesteps 2, 5,10, 20, 30, ..., 140. Each timesteps is of the order of 5×10^5 yr. The filled sources symbols are for ULIRGs and MM sources, the open squares are LIRGs/starbursts and the crosses represent evolved starburst as discussed below. The crosses correspond to the grey symbols in Figs. 6–9.

scale than the PDR, and will therefore suffer more from beam dilution (Schleicher et al. 2010). Therefore, even a single AGN embedded in a starburst environment would not likely cause a measurable boost of the HCN line strength. Additionally, HCN enhancement at the highest FIR luminosities due to IR pumping would still not preclude a smooth variation of the HCN strength during a starburst.

In the following discussion the ratio of the high-density and low-density components of the ISM will be used to indicate the sequence of evolutionary time based on the simulation of Sect. 2.1. The emission of the low-density component is well represented by CO (1−0), which is less affected by a nuclear starburst because it originates in a region much larger than the starburst region. Consequently, the HCN (1−0)/CO (1−0) ratio may serve as a indicator of the relative HD depletion over time.

A simple test of the viability of HCN (1−0)/CO (1−0) as an indicator of the (progressing) evolutionary time may be the comparison in Fig. 4 of the distribution of the ratios of the sources used in the discussions below (no upper limits; see Table 2) with

Table 2. Transitional line ratios for high-density tracer molecules.

Source IRAS	Name	$\frac{\mathrm{HCN\,(1-0)}}{\mathrm{CO\,(1-0)}}$	$\frac{\mathrm{HNC\,(1-0)}}{\mathrm{HCN\,(1-0)}}$	$\frac{\mathrm{HCO^+\,(1-0)}}{\mathrm{HCN\,(1-0)}}$	$\frac{\mathrm{CN\,(1-0)}}{\mathrm{HCN\,(1-0)}}$	$\frac{\mathrm{CN\,(2-1)}}{\mathrm{HCN\,(1-0)}}$	$\frac{\mathrm{CN\,(2-1)}}{\mathrm{CN\,(1-0)}}$	$\frac{\mathrm{CS\,(3-2)}}{\mathrm{HCN\,(1-0)}}$
00450−2533	NGC 253	–1.41 (–2.768)	–0.13 (–1.406)	–0.06 (–1.234)	0.24 (–0.805)	0.11 (–1.129)	–0.13 (–1.190)	–0.39 (–1.366)
01053−1746	IC 1623	–1.44 (–2.249)	...	0.06 (–0.731)	...	...	...	...
01403+1323	NGC 660	–1.34 (–1.778)	–0.24 (–0.649)	–0.00 (–0.502)	<–0.58	...	...	<0.42
01484+2220	NGC 695	–1.84	...	0.20	...	...	...	...
02193+4207	NGC 891	–1.77 (–2.325)	–0.30 (–0.749)	0.05 (–0.267)	...	...	...	...
02401−0013	NGC 1068	–1.08 (–2.196)	–0.41 (–1.197)	–0.04 (–1.038)	0.26 (–0.683)	...	...	–0.49 (–1.297)
03317−3618	NGC 1365	–1.21 (–1.521)	–0.43 (–0.709)	–0.18 (–0.422)	...	...	...	–0.45 (–0.727)
03419+6756	IC 342	–1.56 (–2.800)	–0.47 (–1.658)	–0.29 (–1.221)	–0.10 (–1.154)	–0.59 (–1.747)	–0.49 (–1.606)	–0.61 (–1.409)
04315−0840	NGC 1614	–1.53 (–2.784)	...	...	0.35 (0.051)	0.45 (–0.245)	0.10 (–0.167)	...
05059−3734	NGC 1808	–1.25 (–2.315)	–0.37 (–1.000)	–0.26 (–1.376)	–0.02 (–1.292)	–0.12 (–1.282)	–0.10 (–1.345)	–1.03 (–1.474)
05083+7936	VII Zw 31	–1.31	...	–0.15	...	...	...	...
05414+5840	...	–1.44 (–2.211)	<–0.59	–0.21 (–0.690)	–0.11 (–0.878)	<–0.16	<–0.05	<0.20
06106+7822	NGC 2146	–1.87 (–3.381)	–0.32 (–1.045)	0.10 (–0.674)	0.31 (–0.289)	...	...	<–0.23
07160−6215	NGC 2369	–1.37 (–1.841)	<–0.24	...	...	...	...	<–0.06
09293+2143	NGC 2903	–1.62 (–2.316)	–0.63 (–1.166)	–0.44 (–0.906)	...	...	...	...
09517+6954	M 82	–1.59 (–2.690)	–0.28 (–1.321)	0.20 (–0.860)	0.14 (–0.736)	–0.13 (–1.144)	–0.27 (–1.196)	–0.20 (–0.961)
09585+5555	NGC 3079	–1.61 (–2.299)	–0.13 (–0.723)	<–0.66	...	...	...	–0.45 (–0.979)
10257−4338	NGC 3256	–1.42 (–2.142)	<–0.04	0.11 (–0.549)	–0.16 (–0.869)	–0.31 (–0.992)	–0.16 (–1.157)	<–0.15
11143−7556	NGC 3620	–1.12 (–1.490)	<–0.45	<–0.28	...	...	...	–0.05 (–0.387)
11176+1351	NGC 3628	–1.68 (–2.301)	–0.23 (–0.803)	–0.21 (–0.740)	...	...	...	...
11257+5850a	Arp 299a	–1.38 (–2.190)	–0.38 (–0.925)	0.21 (–0.523)	–0.14 (–0.670)	...	...	<–0.05
11257+5850bc	Arp 299bc	–1.32 (–2.361)	...	–0.10	0.45 (–0.244)	...	...	...
11506−3851	...	–0.74 (–1.333)	<–0.25	<–0.49	...	...	...	–0.37 (–0.833)
12112+0305	...	–1.13	...	–0.22	...	...	...	...
12243−0036	...	–1.10 (–2.017)	0.01 (–0.756)	–0.13 (–0.816)	–0.14 (–0.794)	<0.09	<0.24	0.09 (–0.620)
12540+5708	Mrk 231	–0.77	–0.16 (–0.860)	–0.41	–0.12 (–0.518)	–0.64 (–1.199)	–0.52 (–0.833)	...
12542+2157	NGC 4826	–1.89 (–3.065)	...	–0.23 (-1.374)	...	...	...	...
13025−4911	NGC 4945	–1.37 (–3.114)	–0.27 (–1.863)	0.03 (–1.675)	0.26 (–1.257)	0.16 (–1.496)	–0.10 (–1.647)	–0.18 (–1.823)
13126+2452	...	<–1.92	...	>0.23	...	>0.04	...	...
13183+3423	Arp 193	–1.54	...	0.28	...	...	...	...
13341−2936	M 83	–0.98 (–1.483)	–0.53 (–1.030)	–0.35 (–0.640)	...	...	...	–1.09 (–1.491)
13428+5608	Mrk 273	–0.79	<–0.41	–0.42	<–0.37	...	...	...
15065−1107	...	–1.77 (–2.269)	...	...	...	...	...	<–0.02
15107+0724	...	–0.96 (–1.510)	–0.27 (–0.440)	–0.30 (–0.651)	–0.24 (–0.114)	<0.32	<0.56	–0.04 (–0.441)
15327+2340	Arp 220	–1.05 (–2.440)	–0.12 (–0.786)	–0.32 (–1.259)	0.18 (–0.628)	–0.06 (–0.574)	–0.24 (–0.711)	0.10 (–0.538)
16504+0228	NGC 6240	–1.03	–0.59 (–0.894)	–0.13	–0.32 (–1.161)	0.13 (–0.981)	0.45 (–0.340)	<–0.07
17208−0014	...	–1.14	...	–0.17	<0.09	<–0.28	...	...
20338+5958	NGC 6946	–1.49 (–3.484)	–0.39 (–1.516)	–0.07 (–1.874)	...	...	...	–0.72 (–1.098)
21453−3511	NGC 7130	–1.19 (–2.470)	–0.22 (–1.121)	...	–0.09 (–0.786)	0.05 (–0.906)	0.14 (–0.505)	...
22025+4205	...	–0.82 (–1.611)	<–0.29	–0.38 (–0.821)	<–0.42	<–0.22	...	...
22347+3409	NGC 7331	>–1.61	...	<–0.22	...	...	...	...
23007+0836	NGC 7469	–1.41	0.20 (–0.650)	0.17	0.30 (–0.607)	...	...	...
23134−4251	NGC 7552	–1.28 (–1.917)	–0.33 (–0.754)	–0.05 (–0.597)	...	...	...	–0.19 (–0.747)
23156−4238	NGC 7582	–1.52 (–2.051)	<0.09	0.13 (–0.216)	...	...	...	<0.04
23365+3604	...	–1.26	...	–0.21	...	...	...	...
23488+1949	NGC 7771	–1.34	...	–0.02	...	...	...	...
23488+2018	Mrk 331	–1.54	...	0.10	...	...	...	...

Notes. The ratios are given in logarithmic form.

the shape of the predicted curves in Fig. 1d (see Sect. 2.1). While the sample is incomplete at lower $L_{\mathrm{HCN}}/L_{\mathrm{CO}}$ values, this simple model agrees quite well with observations although the vertical scaling is still unknown.

A second test of the use of HCN (1−0)/CO (1−0) as evolutionary time indicator is a comparison in Fig. 5 of the ratios versus the FIR-luminosity with the predictions made in Fig. 1c (see Sect. 2.1). The locations of the data points are consistent with them following the predicted evolutionary curves. Assuming that the preliminary model in Sect. 2.1 depicts the first-order evolutionary behavior of a starburst, the location of data points relative to the evolutionary curves would be an indication of the evolutionary age of the starburst. Evolutionary ages are indicated by dotted lines covering a period of 10^8 yr. More detailed models need to be constructed to accurately apply this concept to the evolution of a starburst.

3. Signatures of evolution of the molecular ISM

A molecular line ratio indicates changes in the chemical and physical environment that may affect both molecules in a different manner. The line ratios for a number of characteristic molecular transitions have been presented as a function of the HCN (1−0)/CO (1−0) line ratio in Figs. 6–9. The line ratios

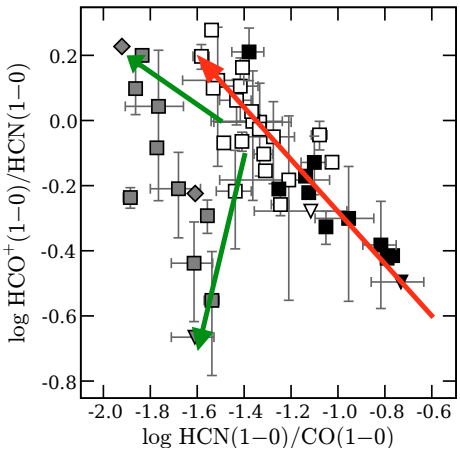

Fig. 6. The ratio of HCO^+ (1−0)/HCN (1−0) versus the HCN (1−0)/CO (1−0). The variation of HCO^+ compared with the variation of the ratio of another high-density and a low-density tracer. The data points are squares for reliable values or triangles for upper and lower limits. Filled symbols indicate ULIRGs and OH MM sources in the sample. The open symbols represent LIRGs/starbursts. The sources with grey symbols are at later stages of starburst evolution (corresponding to crosses in Fig. 5). The red arrow designates the predicted effect of density variation and the green arrows designate the predicted effect of feedback through mechanical heating as simulated in Fig. 2.

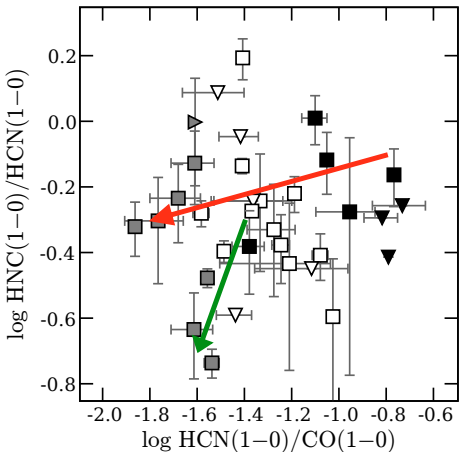

Fig. 7. The ratio of HNC (1−0)/HCN (1−0) versus the HCN (1−0)/CO (1−0) ratio. The ratio of HCN/CO represents the progression of time for the nuclear activity running from right to left. The symbols and colors are as in Fig. 6.

for high-density tracers in Table 2 are from Baan et al. (2008) with some corrections of the calibration for some literature data. The high-luminosity ULIRGs and OH Megamasers (OH MM), which are at early stages of evolution, are located on the right-hand side of the diagrams (filled symbols). Evolved sources at lower $L_{\rm FIR}$ (grey symbols) are located on the left of the diagrams and may have been affected by feedback during these late stages of evolution (see Sect. 3.1 below).

The diagrams display a systematic move towards lower $L_{\rm HCN}/L_{\rm CO}$ values in the diagram as a result of the evolution of the starburst. Any spread of the observed line ratios (along y-axis) would result from variation of environmental effects and excitation conditions.

3.1. The HCO^+/HCN – HCN/CO relation

The diagram of the HCO^+ (1−0)/HCN (1−0) data (Fig. 6) displays two well-defined distributions of data points which are both decreasing along the HCN (1−0)/CO (1−0) axis (see Baan et al. 2008, for a first version). The main distribution contains ULIRGs and luminous starburst galaxies while the second group consists of low FIR luminosity sources that have been affected by feedback (see below). Both distributions suggests a steady increase of the HCO^+ (1−0)/HCN (1−0) ratio with time, while the strength of both transitions decreases during the evolution of the outburst.

The HCO^+ (1−0)/HCN (1−0) ratio in PDR-dominated environments is predominantly sensitive to the mean density of the medium. At higher densities it decreases because of the increased dissociative recombination rate of HCO^+ with free electrons. At lower molecular densities and at later stages of starburst evolution, the enhanced ionization balance ($F_{\rm UV}/n$) would enhance HCO^+, while at $n \leq 10^4$ cm^{-3} the increased cosmic ray flux resulting from the SN of massive stars again destroys HCO^+.

Modeling of the predicted effect of changing the average density of the ISM show a significant increase of the HCO^+ (1−0)/HCN (1−0) ratio for a change in density from $10^{5.5}$ to 10^4 cm^{-3} (Fig. 2). This trend agrees with the general trend of the data points as shown by the red arrow in Fig. 6.

Feedback by mechanical heating at a lower density of 10^4 cm^{-3} lowers the HCO^+ (1−0)/HCN (1−0) ratio at the cloud centers (by a factor of three), but it is complicated by the mixed effects of an increasing temperature and a decreasing density. Feedback modeling results in Fig. 2 suggest a displacement of the HCO^+ (1−0)/HCN (1−0) data points towards lower values that depends on feedback intensity (in between two green arrows). This would move sources from the main distribution towards the distribution of evolved sources (filled grey symbols at the left side of Fig. 6).

Modeling shows that higher HCO^+/HCN values may also result from the presence of an AGN and the creation of dominant XDRs (Loenen et al. 2008). However, this change would be accompanied by an increase in the HNC/HCN ratios, which is not observed in the data. It should be noted that the separation of the evolved sources from the main body would indicates that the nuclear feedback conditions vary on very short timescales.

The main distribution of data points in the HCO^+/HCN diagram is consistent with the predictions for a systematic change of the line ratio towards lower HCN/CO values resulting from environmental changes during the evolution of a starburst. A second group of data points for evolved sources, which display the effects of feedback, displays a different dependence for the HCO^+/HCN ratio on evolutionary time.

3.2. The HNC/HCN – HCN/CO relation

The HNC (1−0)/HCN (1−0) ratio displays data points covering a large range of values (factor of 8; Fig. 7). However, it should be noticed that data points for ULIRGs and also for evolved galaxies are separated from the central distribution (forming three bands of points). The distribution of data points displays a weak overall decrease with decreasing HCN/CO by a factor of 1.6.

The HNC (1−0)/HCN (1−0) ratio is sensitive to the heating of the environment (Loenen et al. 2008). For values larger than unity, the dominant heating source would be X-rays in XDRs. NGC 7469, with the largest ratio in our sample, is known to have a circum-nuclear starburst and a black hole X-ray source. Alternatively to X-ray heating, the enhancement in these sources may be caused by pumping with a very warm FIR radiation

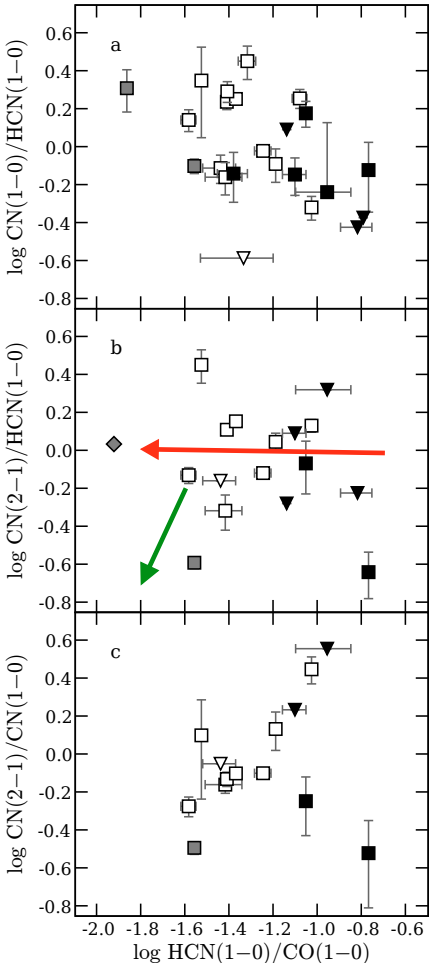

Fig. 8. The CN (1−0)/HCN (1−0) and CN (2−1)/HCN (1−0) ratios versus the HCN (1−0)/CO (1−0) ratio. Frame c) presents the CN (2−1)/CN (1−0) line ratio. The symbols and colors are as in Fig. 6.

field that dominates over the collisional processes for densities up to 10^6 cm^{-3} (Aalto et al. 2007). This process would operate at early stages of the evolution with high densities and intense IR radiation fields, which could explain the apparent HNC/HCN over-luminosity of the distinct group of OH MM/ULIRG sources in Fig. 7 (l.t.r.: NGC 4418, Arp 220, IRAS 15107+0724, and Mrk 231).

For HNC (1−0)/HCN (1−0) ratios in the range of 0.5 to unity, the dominant heating source is the UV radiation in young PDRs. Ratios smaller than 0.5 can not be explained by the steady state models of PDRs (and XDRs). In a study of additional heating sources, Meijerink et al. (2006) found that cosmic ray heating is not sufficient to influence the HCN and HNC abundances. On the other hand, an increase in the temperature by means of SNe and SNR shocks will decrease the HNC/HCN ratio, by opening an additional chemical conversion path from HNC to HCN (Schilke et al. 1992). This conversion of HNC at later stages of evolution of the starburst is facilitated by turbulent heating of gas in the central and densest regions of the ISM and is a temperature ($T \geq$ 100 K) dependent chemical process (Loenen et al. 2008).

The simulations from Sect. 2.2 show that the HNC/HCN ratio would systematically decrease with a factor 1.6 when the average density drops from $10^{5.5}$ to 10^4 cm^{-3} as depicted with the red arrow. This arrow is representative of the average response of the emission regions with the highest column densities and agrees with the observed average value for the ratio of around 0.6. With mechanical heating, the HNC/HCN ratio may be reduced by as much as 2.5 at smaller HCN/CO values as depicted with the green arrow. The onset of the effects of mechanical feedback would vary with the type of galaxy and the intensity of the starburst. The general distribution of data points is consistent with the changes expected for the line ratio as a result of the lowering of density and the introduction of mechanical heating from feedback.

The HNC/HCN diagram displays three apparent groups of data points making a large (vertical) spread of the line ratio and possibly suggests enhanced ratios for the high-luminosity ULIRGs (see discussion above). The group of evolved sources at low HCN/CO forms a separate group of sources that shows little variation with time. While the red and green arrows depict the average time behavior of the distribution, the vertical spread and the grouping suggest that additional physics affects the HNC/HCN line ratios. Nevertheless, the HNC/HCN would also show a (weak) systematic variation with evolutionary time until feedback changes the environment.

3.3. The CN/HCN – HCN/CO relation

The variation of the two CN/HCN ratios versus the HCN/CO ratio are presented in Fig. 8. The CN (1−0)/HCN (1−0) ratio (Fig. 8a) displays a distribution that increases with decreasing HCN/CO ratios. On the other hand, the CN (2−1)/HCN (1−0) distribution (frame b) shows twice the spread of the CN (1−0)/HCN (1−0) ratio with a consistently zero slope.

The CN emission is generally enhanced in PDR-dominated Galactic (Greaves & Church 1996; Rodriguez-Franco et al. 1998) and extra-galactic environments (Fuente et al. 2005). To a large extent, CN is a photo-dissociation product of HCN and HNC in the irradiated outer layers of molecular clouds and serves as a diagnostic of the FUV and cosmic-ray driven gas-phase chemistry (see Rodriguez-Franco et al. 1998; Boger & Sternberg 2005).

The gradual increase in the CN (1−0)/HCN (1−0) ratio results from the relatively low critical density of the CN (1−0) transition (similar to HCO$^+$ (1−0)). As the average density drops, the CN (1−0) line strength at lower column densities will become enhanced and less thermalized. In addition, the CN (2−1) emitting volume (towards cloud centers) reduces relative to the CN (1−0) emitting surface regions (low-column density) during the outburst.

The abundance simulations of PDR-dominated emission regions show that the CN/HCN abundance ratio in regions with high column densities remains close to unity when lowering the density from $10^{5.5}$ to 10^4 (Fig. 2). Radiation transfer calculations have not yet been done for CN. This absence of variation of the CN abundance is consistent with the CN (2−1)/HCN (1−0) data points in Fig. 8b (red arrow). The introduction of mechanical heating due to feedback at later evolutionary times (green arrow) would lower the relative abundance by as much as a factor of 20, which is not yet seen in the data.

Inspection of the data points in Fig. 8a, b shows that two luminous ULIRG sources, Arp 220 and Mrk 231, have an enhanced CN (1−0) transition and a reduced CN (2−1) transition. This also shows in the line ratios in Fig. 8c. This apparent lowering of the T_{ex} may be result from peculiar pumping conditions in very luminous ULIRGs, possibly related to the anomalous FIR pumping of HNC in these same sources (Aalto et al. 2007).

Assuming that the two ULIRG sources are indeed subject to anomalous conditions, the CN (1−0)/HCN trend would be more upwards and the CN (2−1)/HCN trend would be slightly

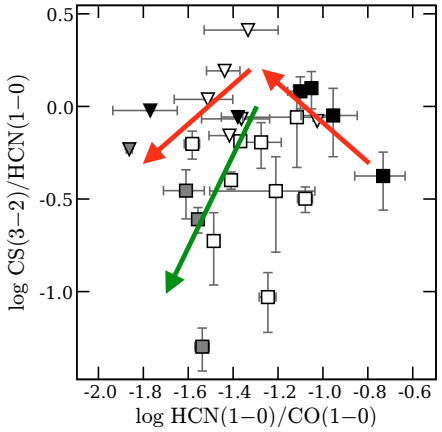

Fig. 9. The ratios of CS (3−2)/HCN (1−0) versus the HCN (1−0)/CO (1−0) ratio. The symbols and colors are as in Fig. 6.

downward with decreasing HCN/CO. In addition, without these data points the observed CN (2−1)/CN (1−0) ratio (Fig. 8c) displays a (nearly) linear dependence for the regular starbursts and LIRGs with HCN/CO and evolutionary age. Since the abundance of CN remains relatively constant, this factor 10 variation in the line ratio could be attributed to excitation effects or variation of the density. Attributing this change to (excitation) temperature only suggests a change in effective T_{ex} from 20 to 9 K, which is rather implausible. Although this relation is still tentative because of the small number of data points, this line ratio could be an indicator of the changing density and the difference in critical densities of the two lines.

The CN/HCN diagrams suggest a systematic increase of the CN (1−0)/HCN (1−0) ratio with evolutionary time accompanied by no-change for the CN (2−1)/HCN (1−0) ratio. This would result in a (density-related) systematic lowering of the CN (2−1)/CN (1−0) ratio with evolutionary time. Detailed modeling of CN line ratios (in progress) is required to explain the environmental influence on the ratios in ULIRGs and the effect of feedback in evolved starbursts.

3.4. The CS/HCN – HCN/CO relation

The CS (3−2)/HCN (1−0) diagram (Fig. 9) also displays a large spread in data points (factor 30) and shows band-like sub-structure similar to the HNC (1−0)/HCN (1−0) diagram of Fig. 7. Again the OH MM/ULIRG sources form the upper envelope with enhanced CS (3−2) emission. The diagnostic diagram of the CS (3−2)/HCN (1−0) ratio displays a downward trend going to lower HCN/CO values during the course of an outburst.

The observed CS (3−2)/HCN (1−0) ratios mostly lie below unity, which is slightly lower than predicted from modeling (Fig. 2). These lower ratios may indicate that the average Sulfur-depletion in the sources is somewhat higher than the value of 400 used for Fig. 2c (see Loenen et al. 2010).

As a density tracer to first order with a high critical density, the CS emissions depend strongly on the clumped high-density regions with the highest column density in the ISM. The lower density (outer) regions of molecular structures contribute little to the overall emission (see also Fig. 2c). CS may be enhanced in photon-dominated regions due to reactions involving S^+ (Sternberg & Dalgarno 1995), while an enhanced cosmic ray flux would deplete its abundance.

The modeling results show that the average CS (3−2)/HCN (1−0) line ratio at high column density would first increase when the average density drops to 10^5 cm^{-3} and then decrease again (or flatten) when it reaches 10^4 cm^{-3} (Fig. 2). The introduction of mechanical heating and feedback at 10^4 cm^{-3} would lower the ratio by a factor up to 10. These theoretical tendencies have been indicated in Fig. 9 with two red arrows (for density) and a green arrow (for feedback).

The CS/HCN diagram also displays three apparent groups of data points making a large (vertical) spread of the line ratio, similar to the HNC/HCN diagram. Again there is the suggestion of enhanced ratios for the high-luminosity ULIRGs. The group of evolved sources at low HCN/CO also shows little variation with time. While the red and green arrows depict the average time behavior of the distribution, the vertical spread and the grouping suggest that additional physics affects the CS/HCN line ratios and results in a (weak) systematic variation with evolutionary time until feedback changes the environment.

4. Summary

The evolutionary stages of a nuclear starburst represent a well-determined sequence of events that would affect the ISM in a complex but predictable manner. As a result, the characteristics of the ISM and the subsequent star-formation process will change systematically during the course of the outburst and ultimately leads to the termination of the process. The dominant effects describing the nuclear ISM are the steady depletion of the high-density molecular component, the decreasing average density of the high density medium, and the increasing temperature resulting from the heating due to feedback.

A simple model has been discussed that describes the decreasing high-density component of the ISM during an outburst. It has also been argued that HCN is the molecular species that is least affected by the chemical and physical changes in the ISM and best serves as an indicator of the high-density component in the ISM. For this reason, all molecular variations in this study are measured relative to the strength of the HCN (1−0). Molecular species will react differently to the changing environment of the nuclear ISM and these molecules will reveal different aspects of the changing physical and chemical environment. In this example, the decreasing HCN (1−0)/CO (1−0) ratio serves as an initial measure of evolutionary time for the starburst. Systematic changes may be seen for all characteristic line ratios with evolutionary time. The observed ratios with HCN (1−0) for the two transitions with lower critical densities, CN (1−0) and HCO^+ (1−0), display a systematic increase with evolutionary time of the starburst. Furthermore, the CN (2−1)/CN (1−0) ratio for starbursts and LIRGs (tentatively) decreases systematically with evolutionary time. All these ratios may be used as indicators of evolutionary time of the starburst.

The two other transitions with higher critical densities, HNC (1−0) and CS (3−2) display a more complicated picture because it appears that additional physical processes affect the ratios, particularly for the highest-luminosity ULRGs. Both transitions display weak evolutionary variation with evolutionary age. While FIR pumping may account for the anomalous HNC/HCN ratio in these ULIRGs, a pumping mechanism for CS has yet to be identified. Besides HNC and CS, CN also displays anomalous excitation during the early ULIRG stage. Here the CN (1−0) line is enhanced and the CN (2−1) line is reduced relative to HCN (1−0), which may reduce the CN (2−1)/CN (1−0) ratio during early stages of evolution.

In addition to the main group of sources that display a systematic increase in the observed ratios with a lowering of the HCN/CO ratio, a group of evolved sources has been identified that would display a different dependence on evolutionary time. Besides the systematic lowering of density in the PDR-dominated environment (from $10^{5.5}$ to 10^{4} cm^{-3}), the feedback from SNe and SNRs during later stages of evolution provides mechanical heating leads to lower ratios for all line ratio with respect to HCN (1−0) (Loenen et al. 2008).

The observed variation of characteristic line ratios may be used to diagnose the evolutionary state of the nuclear activity in galaxies. This would allow to establish an evolutionary sequence for ULIRGs and (future) SMGs and a way to understand and diagnose their physical processes. The systematic changes of the characteristic molecular line ratios already provide a first view of evolutionary sequence for the nuclear activity. While the relation between the HCN (1−0)/CO (1−0) line ratio and evolutionary time only provides relative time during the evolution of the starburst, further modeling of the observed changes would provide a more accurate translation to evolutionary time. In addition, sequential modeling to reconstruct the changing nuclear environment will provide a better understanding and identification of the different physical and chemical processes that determine the evolution of the molecular environment during a nuclear outburst. Additional observational data of multiple molecular transitions will further improve the understanding of the complex myriad of competing processes.

References

Aalto, S., Spaans, M., Wiedner, M. C., & Hüttemeister, S. 2007, A&A, 464, 193
Baan, W. A., Henkel, C., Loenen, A. F., Baudry, A., & Wiklind, T. 2008, A&A, 477, 747
Bergin, E. A., Neufeld, D. A., & Melnick, G. J. 1998, ApJ, 499, 777
Boger, G. I., & Sternberg, A. 2005, ApJ, 632, 302
Coziol, R. 1996, A&A, 309, 345
Curran, S. J., Aalto, S., & Booth, R. S. 2000, A&AS, 141, 193
Fuente, A., García-Burillo, S., Gerin, M., et al. 2005, ApJ, 619, L155
Gao, Y., & Solomon, P. M. 2004, ApJS, 152, 63
Graciá-Carpio, J., García-Burillo, S., Planesas, P., & Colina, L. 2006, ApJ, 640, L135
Graciá-Carpio, J., García-Burillo, S., Planesas, P., Fuente, A., & Usero, A. 2008, A&A, 479, 703
Greaves, J. S., & Church, S. E. 1996, MNRAS, 283, 1179
Lepp, S., & Dalgarno, A. 1996, A&A, 306, L21
Loenen, A. F., Baan, W. A., & Spaans, M. 2006, A&A, 458, 89
Loenen, A. F., Baan, W. A., & Spaans, M. 2007, in IAU Symp., 242, 462
Loenen, A. F., Spaans, M., Baan, W. A., & Meijerink, R. 2008, A&A, 488, L5
Loenen, A. F., Baan, W. A., & Spaans, M. 2010, A&A, submitted
Meijerink, R., & Spaans, M. 2005, A&A, 436, 397
Meijerink, R., Spaans, M., & Israel, F. P. 2006, ApJ, 650, L103
Papadopoulos, P. P. 2007, ApJ, 656, 792
Rodriguez-Franco, A., Martin-Pintado, J., & Fuente, A. 1998, A&A, 329, 1097
Schilke, P., Walmsley, C. M., Pineau Des Forets, G., et al. 1992, A&A, 256, 595
Schleicher, D. R. G., Spaans, M., & Klessen, R. S. 2010, A&A, 513, A7
Schöier, F. L., van der Tak, F. F. S., van Dishoeck, E. F., & Black, J. H. 2005, A&A, 432, 369
Spaans, M. 1996, A&A, 307, 271
Spaans, M., & van Dishoeck, E. F. 1997, A&A, 323, 953
Sternberg, A., & Dalgarno, A. 1995, ApJS, 99, 565